Magnetic Helicity in Emerging Solar Active Regions

Y. Liu[1], J. T. Hoeksema[1], M. Bobra[1], K. Hayashi[1], P. W. Schuck[2], X. Sun[1]

ABSTRACT

Using vector magnetic field data from the Helioseismic and Magnetic Imager (HMI) instrument aboard the Solar Dynamics Observatory (SDO), we study magnetic helicity injection into the corona in emerging active regions and examine the hemispheric helicity rule. In every region studied, photospheric shearing motion contributes most of the helicity accumulated in the corona. In a sample of 28 emerging active regions, 17 active regions follow the hemisphere rule (61% ± 18% at a 95% confidence interval). Magnetic helicity and twist in 25 active regions (89% ± 11%) have the same sign. The maximum magnetic twist, which depends on the size of an active region, is inferred in a sample of 23 emerging active regions with a bipolar magnetic field configuration.

Subject headings: Sun: interior—Sun: photosphere—Sun: magnetic fields—Sun: sunspots

1. Introduction

Magnetic helicity, $H = \int_V (\mathbf{A} \cdot \mathbf{B}) dv$ with $\mathbf{A}$, the vector potential, and $\mathbf{B}$, the magnetic field, is sometimes used to describe the complexity of a solar active region (AR) (e.g. Démoulin 2007). Helicity in a volume V is gauge invariant only when no magnetic flux penetrates the surfaces of V. Because magnetic field in active regions penetrates the photosphere, a gauge-invariant relative helicity, $\Delta H = \int_V (\mathbf{A} \cdot \mathbf{B} - \mathbf{A}_R \cdot \mathbf{B}_R) dv$, must be used for estimating the helicity (Berger & Field 1984). $\mathbf{B}_R$ is a reference magnetic field and $\mathbf{A}_R$ is vector potential. Usually, the potential field, $\mathbf{B}_p$, is chosen as the reference field. It has the same vertical field on the photosphere. For simplicity, hereafter we do not generally distinguish between magnetic helicity and relative magnetic helicity.

[1]W. W. Hansen Experimental Physics Laboratory, Stanford University, Stanford, CA94305-4085

[2]Space Weather Laboratory, Code 674, Heliophysics Science Division , NASA Goddard Space Flight Center, Greenbelt, MD 20771

One way to measure the helicity in an AR is to integrate over time the helicity flux across the photosphere. The relative helicity flux (helicity flux hereafter) across a surface S can be computed with the following equation (Berger 1984),

$$\left.\frac{dH}{dt}\right|_S = \Big[2\int_S (\mathbf{A}_p \cdot \mathbf{B}_t) V_{\perp n} dS\Big]_{(emergence-term)} - \Big[2\int_S (\mathbf{A}_p \cdot \mathbf{V}_{\perp t}) B_n dS\Big]_{(shear-term)}, \quad (1)$$

where $\mathbf{A}_p$ is the vector potential of the potential field $\mathbf{B}_p$; $\mathbf{B}_t$ and B_n denote the tangential and normal magnetic fields; and $\mathbf{V}_{\perp t}$ and $\mathrm{V}_{\perp n}$ are the tangential and normal components of velocity $\mathbf{V}_\perp$, the velocity perpendicular to magnetic field lines. The first term represents the helicity flux across the surface S due to advection of twisted magnetic flux tubes (the emergence term hereafter). The second term is due to photospheric motions that shear and braid the field lines (the shear term hereafter) (Berger 1984; Kusano et al. 2002; Nindos et al. 2003; Pevtsov et al. 2003; Pariat et al. 2005; Démoulin 2007). In a previous study we analyzed two active regions (ARs) and found that both terms inject into the corona helicity of the same sign and the shear term contributes most of the helicity during the emergence (Liu & Schuck 2012). This is the opposite of what Kusano et al. (2002) found in another emerging AR, where the helicities from the two terms are comparable but have opposite signs (see also, Yamamoto & Sakurai 2009). A survey study is needed to examine this discrepancy.

The kinetic helicity in the convection zone (CZ) is believed to change its sign across the solar equator due to the Coriolis force. The magnetic helicity is expected to change its sign too, because the flow drags field lines with it (Gilman 1983). Proxies of magnetic helicity have been proposed and used to search for a hemispheric sign preference (hemisphere rule hereafter) (for a review see, e.g., Pevtsov & Balasubramaniam 2003). Using the constant force-free α as a proxy for magnetic twist, a fraction of magnetic helicity, Seehafer (1990) calculated α for 16 ARs and found that the sign of α is hemisphere dependent: negative in the northern hemisphere and positive in the southern hemisphere. Pevtsov et al. (1995) calculated a similar proxy, α_{best}, for 69 ARs, and found that 75% of ARs in the northern hemisphere and 69% of ARs in the southern hemisphere follow the hemisphere rule (see also, e.g., Hagino & Sakurai 2004; Zhang et al. 2010; Hao & Zhang 2011). α_{best} is a single force-free α determined for an AR by minimizing the difference between the tangential field of the resulting linear force-free field and the observed field. A force-free field satisfies $\bigtriangledown \times \mathbf{B} = \alpha \mathbf{B}$, where $\mathbf{B}$ is magnetic field and α is a scalar quantity that depends on position. For a linear force-free field, α is constant.

Bao & Zhang (1998) computed a different proxy of magnetic helicity: ρ, the imbalance of partial current helicity density. ρ, introduced by Abramenko et al. (1996), is defined as $\sum h_{cz} / \sum \mid h_{cz} \mid \times 100\%$, where the current helicity density $h_{cz} = B_z(\bigtriangledown \times \mathbf{B})_z$. Bao & Zhang reported 84% of ARs in the northern hemisphere and 81% of ARs in the southern

hemisphere obey the hemisphere rule. Neither α nor ρ are true measures of magnetic helicity, though it has been theoretically demonstrated that, *in a linear force-free field*, the magnetic helicity has the same sign as the constant force-free α and the current helicity (Berger 1985; Georgoulis & LaBonte 2007).

Attempts to examine the hemisphere rule using magnetic helicity in ARs have been made by LaBonte et al. (2007), Yang et al. (2009), and Zhang & Yang (2013). LaBonte et al. (2007) measured helicity flux across the photosphere in 393 ARs. They found 57% of ARs in the northern hemisphere inject negative helicity and 60% of ARs in the southern inject positive helicity (see also, Zhang & Yang 2013). Yang et al. (2009) measured the magnetic helicity for 58 emerging ARs. The helicity was computed by integrating over time the helicity flux during the entire emergence of the AR. They found 57% of the ARs follow the hemisphere rule. In these studies, the Local Correlation Tracking method (LCT) is applied to the *Michelson Doppler Imager* (MDI; Scherrer et al. 1995) line-of-sight magnetograms to infer the tangential velocity and a hypothesis proposed by Démoulin & Berger (2003) is adapted to estimate the helicity flux. The helicity flux (Equation 1) in their approach is simplified to,

$$\left.\frac{dH}{dt}\right|_S = -2\int_S (\mathbf{A}_p \cdot \mathbf{U}) B_n dS, \tag{2}$$

by introducing the flux transport velocity ($\mathbf{U} = \mathbf{V}_{\perp t} - \frac{V_{\perp n}}{B_n}\mathbf{B}_t$). With the hypothesis proposed by Démoulin & Berger (2003), which argued geometrically that the apparent tangential velocity derived by tracking footpoints of normal magnetic field is in fact the flux transport velocity, the helicity flux is then computed from line-of-sight magnetograms and the aforementioned tracking velocity on the surface. However, Liu & Schuck (2012) demonstrated this method is unable to calculate the helicity completely — it only captures most of the helicity from the shear term, the second term in the right-hand side in Equation (1). A better method is needed to compute both terms that contribute to the coronal helicity. In this investigation, we use Eq. 1 to directly measure the helicity flux across the photosphere for emerging ARs and examine the hemisphere rule. It explicitly takes into account the contributions from both the shear term and the emergence term by using the *Helioseismic and Magnetic Imager* (HMI; Scherrer et al. 2012; Schou et al. 2012) vector magnetic field data (Hoeksema et al. 2013) and a better algorithm for determining the velocity, the Differential Affine Velocity Estimator for Vector Magnetograms (DAVE4VM; Schuck 2008).

Our study will investigate several theoretical relationships between active regions and their magnetic helicity or a helicity proxy, the force-free α parameter. First, we will determine which helicity flux makes a dominant contribution to the coronal helicity: the emergence or shear term. Second, we will examine the hemisphere rule using for the first time direct measurements of the time-integrated helicity flux. These results will be also compared with

the helicity proxy α. Finally, we will examine relationship of α and the active region size. This study will be performed with vector magnetograms from 28 emerging ARs between May 2010 and September 2012 observed by HMI. The helicity flux estimates incorporate contributions from both the shear term and the emergence term by using velocities determined by DAVE4VM.

The paper is organized as follows: Section 2 describes the data. Section 3 describes the analysis of helicity and energy injection in ARs. Section 4 examines the hemisphere rule. We summarize this study in Section 5.

2. Data and Sample

We use vector magnetic field data taken by HMI for this investigation (Hoeksema et al. 2013). The HMI instrument is a filtergraph with a full disk coverage at 4096×4096 pixels. The spatial resolution is about 1" with a 0.5" pixel size. The width of the filter profiles is 76 mÅ. The spectral line is the FeI 6173Å absorption line formed in the photosphere (Norton et al. 2006). The Stokes parameters [I, Q, U, V], measured at 6 wavelength positions and sampled every 720 seconds using a 1350 seconds weighted average in order to suppress the p modes and increase the signal-to-noise ratio, are inverted to retrieve the vector magnetic field using a Milne-Eddington (ME) based inversion algorithm Very Fast Inversion of the Stokes Vector (VFISV; Borrero et al. 2011). The 180° degree ambiguity of the azimuth is resolved using a "minimum energy" algorithm (Metcalf 1994; Metcalf et al. 2006; Leka et al. 2009). The location and extent of the ARs are automatically identified and bounded by a feature recognition model (Turmon et al. 2010), and the disambiguated vector magnetic field data of ARs are deprojected to heliographic coordinates. Here we use a Lambert (cylindrical equal area) projection method centered on the region for remapping. A detailed description of Lambert cylindrical equal area projection method can be found at Sun (2013). For a small area, such as a normal AR, the difference between deprojected maps from different projection methods is small. The impact of this difference on the calculation of helicity flux is evaluated in the next paragraph. The vector velocity field in the photosphere is derived using DAVE4VM applied to the time series of deprojected, registered vector magnetic field data. The window size used in DAVE4VM is 19 pixels. This velocity is further corrected by removing the irrelevant field-aligned plasma flow by,

$$\mathbf{V}_\perp = \mathbf{V} - \frac{\mathbf{V}\cdot\mathbf{B}}{B^2}\mathbf{B}, \tag{3}$$

where $\mathbf{V}_\perp$ is the velocity perpendicular to magnetic field line, and $\mathbf{V}$ is the velocity derived by DAVE4VM. The velocity $\mathbf{V}_\perp$ is used to compute energy and helicity fluxes in this investi-

gation. Detailed information on HMI vector field data processing can be found in Hoeksema et al. (2013).

Usually measurements of an AR on the Sun's surface need to be mapped into a plane for further analysis. Map projections distort the spherical geometry at some level. Depending upon the purpose, various projection methods have been constructed to preserve some of the basic properties, but necessarily distort others. The basic properties include area, shape, direction, distance, and scale. For a typical AR whose size is much smaller than the solar radius, the difference due to applying different projection methods is small. We evaluate the impact this difference could bring to the helicity flux calculation. Shown in Fig. 1 are temporal profiles of helicity flux for active region AR 11158 on 16 February 2011 when it was at S21W37, some distance away from the disk center. Different colors refer to different projection methods applied to the HMI vector magnetic field data. Nine projection methods are tested. Detailed descriptions of the projection methods are available at Snyder (1987). The difference is about 0.36 % on average; the maximum difference is 0.70%. Thus the impact of the projection method is small for helicity calculations. In this investigation we use the Lambert cylindrical equal area projection method.

We choose ARs for which (i) HMI observes the entire course of emergence and (ii) vector magnetic field data are available. In total 28 emerging ARs are selected. The regions appeared between May 2010 and September 2012, the early phase of Solar Cycle 24. 14 ARs were in the northern hemisphere and 14 in the southern. These ARs are summarized in Table 1. Columns 1 and 2 give the NOAA number and latitude of the ARs. The beginning and end of the time interval in which the HMI data are used for this analysis are given in Columns 3 and 4. Usually the start time is before the beginning of emergence of the AR and the stop time is after emergence of the AR ends. The emergence of an AR is determined by identifying the appearance of magnetic feature(s) by examining a movie of B_r over time. The end of the emergence phase of an AR is defined as (1) after the main emergence process, during which the total magnetic flux increases rapidly, and (2) when the increase of the total magnetic flux, if applied, is small in comparison to the increase of the magnetic flux in the main emergence process. These beginning and end times of AR emergence are given in Columns 5 and 6. Column 7 denotes the date for which the data are used to compute α_{av} and r as described in Section 4. Basically, this date is chosen after the AR emergence appears to end. Column 8 provides Hale classification of the ARs (or Mount Wilson Sunspot Magnetic Classification; Hale et al. 1919) for the dates in Column 7. Hale's class data are from NOAA at $http://www.swpc.noaa.gov/ftpdir/warehouse/$.

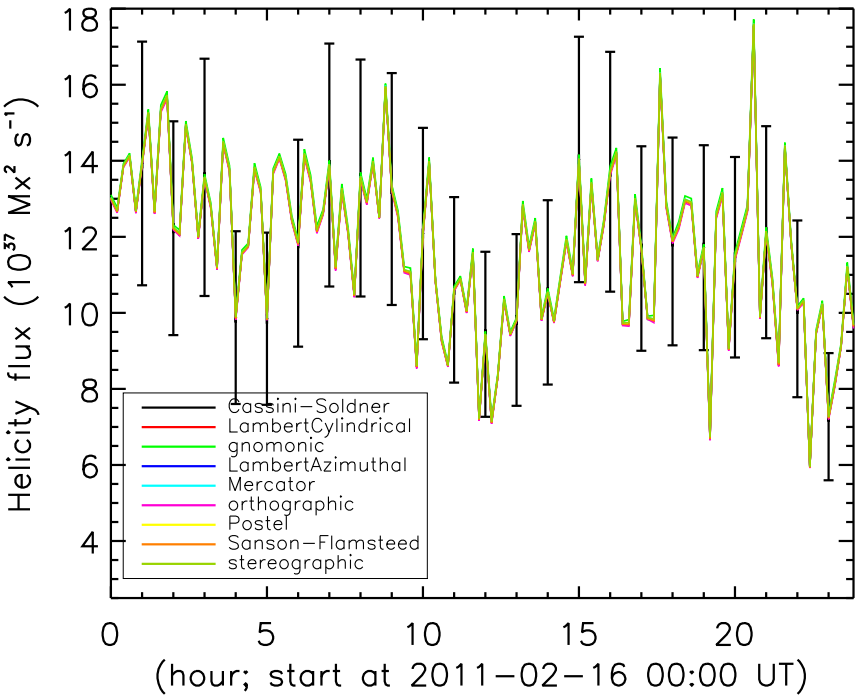

Fig. 1.— Temporal profiles of helicity flux on 16 February 2011 for AR 11158. The region was at S21W37 on 16 February 2011 at 12:00 UT. Different colors refer to the helicity fluxes computed from the vector magnetic field data remapped by different methods. Error bars, reported at several representative times, indicate a 23% uncertainty of helicity flux as estimated by Liu & Schuck (2012). The difference of the resulting fluxes from different methods is less than 0.7%. (The difference is about 0.36% on average, while the maximum is about 0.70%).

3. Helicity and energy injection in ARs during their emergence

We compute magnetic helicity and energy injection into the corona in ARs during their emergence. Similar to the helicity flux, the energy flux across the photosphere S is computed by Kusano et al. (2002) as:

$$\left.\frac{dE}{dt}\right|_S = \left[\frac{1}{4\pi}\int_S B_t^2 V_{\perp n} dS\right]_{(emergence-term)} - \left[\frac{1}{4\pi}\int_S (\mathbf{B}_t \cdot \mathbf{V}_{\perp t}) B_n dS\right]_{(shear-term)}. \quad (4)$$

Energy flux crossing the solar surface comes from emergence of magnetic flux from the solar interior (first term; emergence term) and is generated by shearing magnetic field lines due to tangential motions on the surface (second term; shear term). As an example, Fig. 2 shows

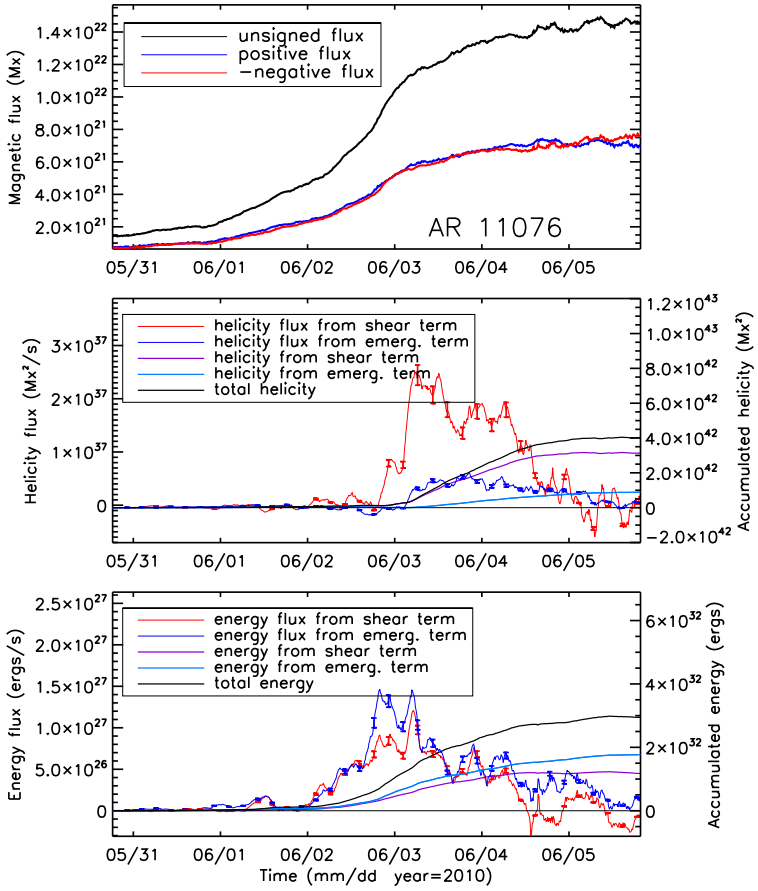

Fig. 2.— Temporal profiles of magnetic fluxes (top), helicity fluxes and helicity (middle), and energy fluxes and energy (bottom) for emerging active region AR 11076 from 31 May 2010 through 05 June 2010. Red and blue curves in the middle and bottom panels represent helicity (middle) and energy (bottom) fluxes across the photosphere from the shear term and emergence term, respectively; purple and light blue curves show the accumulated helicity (middle) and energy (bottom) in the corona from the shear and emergence terms, respectively. The accumulated helicity and energy are calculated by integrating over time the helicity and energy fluxes. The black curves are the helicity (middle) and energy (bottom), i.e. a summation of both terms. A 2-hour running average was applied to the helicity and energy fluxes. Error bars are plotted at representative times based on an uncertainty of 23% for helicity flux and 17% for energy flux estimated by Liu & Schuck (2012). They are further adjusted by the 2-hour running average.

the helicity and energy injected into the corona during the emergence of AR 11076. The panels show temporal profiles of magnetic fluxes (top), helicity fluxes and helicity (middle), and energy fluxes and energy (bottom) from 31 May 2010 to 05 June 2010. Specifics are given in the figure caption. The emergence began on 31 May 2010, and lasted four days. The helicity fluxes from the shear term (red; middle panel) and emergence term (blue; middle panel) began to inject helicity on 2 June 2010 and quickly increased afterwards. The helicity injected into the corona reached $4 \times 10^{42} Mx^2$. The shear term was dominant, contributing 78% of the helicity. Both terms contributed helicity of the same sign. In contrast, energy flux from the shear term (red; bottom panel) was lower than that from the emergence term (blue; bottom panel), contributing 40% of energy. The energy includes both potential energy and free energy.

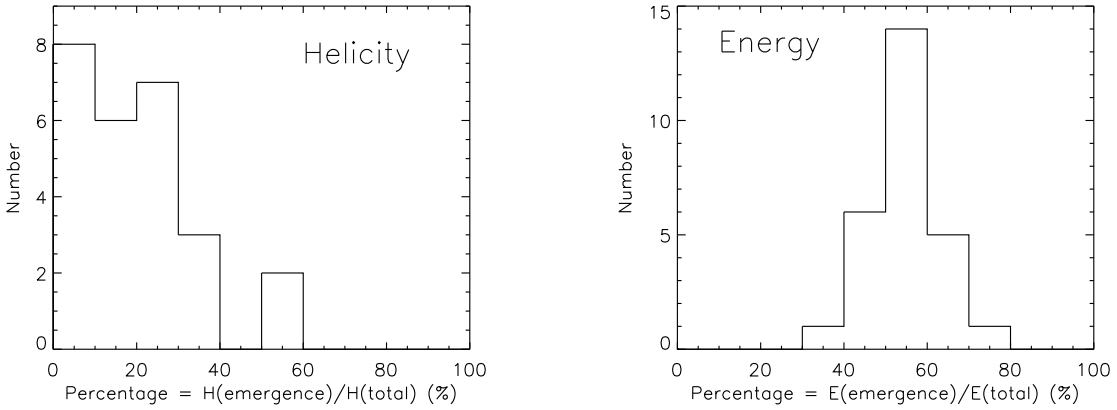

Fig. 3.— Histograms showing the percentage of the emergence term's contribution to the total helicity (left) and energy (right) in the corona for a sample of 26 emerging ARs. The mean value is 14% for helicity and 56% for energy.

A survey study was carried out with a sample of 28 emerging ARs as described in Section 2. The shear term and emergence term inject into the corona helicity of the same sign in 26 of the 28 ARs (93%). The shear term contributes the most helicity; the emergence term contributes slightly more energy (including potential energy and free energy) than the shear term. In the 26 ARs for which the helicities from both terms have the same sign, the emergence term contributes 14% of the helicity and 56% of energy on average. Distributions of the percentage of the emergence term's contribution to the helicity (left) and energy (right) for those 26 ARs are shown in Fig. 3. Two ARs, AR 11161 and AR 11385, injected into the corona helicity of opposite signs. For AR 11161, the shear term contributes 2.97×10^{42} Mx^2 and the emergence term contributes -1.52×10^{42} Mx^2. The contribution of the emergence term turns out to be -105% of the net helicity, though the shear term is still dominant

in terms of the magnitude of the absolute value. If we take the absolute value of both terms, the emergence term contributes 34% of the helicity. For AR 11385, the helicity from the emergence term is 2.19×10^{41} Mx^2 and -1.04×10^{42} Mx^2 from the shear term. The emergence term contributes -27% of the net helicity. If we take absolute values, it is 17%. The shear term contributes the most helicity in those two ARs as well. Therefore, the helicity accumulated in the corona during AR emergence is contributed mainly by the shear term; the energy is contributed approximately equally by both terms, though the emergence term has a slightly higher contribution. An interpretation of this result is given in Liu & Schuck (2012), which is based on the emergence model of a twisted flux tube by Longcope & Welsch (2000). That is, when a highly twisted magnetic tube emerges, only a small fraction of the electric current emerges into the corona. The imbalance between the less twisted emerged field in the corona and highly twisted field in the subsurface leads to surface flows that shear and twist the emerged fields, building up most of the helicity in the corona. In this way, the helicity flux from emergence is low whereas the helicity flux from surface shear flows is dominant. This model is also supported by observation and simulation (e.g. Pevtsov et al. 2003; Fan 2009).

In the sample we studied, it was not uncommon to observe a change in the sign of helicity flux during an AR's emergence. We found that 43% of ARs (12 of 28) changed helicity-flux sign during emergence. Fig. 4 shows such an example. A similar example was reported previously by Yamamoto & Sakurai (2009). They analyzed an emerging active region (AR 8011) and found that the helicity flux of each term changed sign during emergence. They also found that the two terms injected opposite sign helicities (see also, Kusano et al. 2002). In our sample, injection of opposite sign helicity by the two terms is rare — occurring in only two ARs (7%; ARs 11161 and 11385).

4. Examining the hemisphere helicity sign rule

4.1. Testing the hemisphere rule

We examine the hemisphere rule using the same 28 emerging ARs. We take a similar approach as Yang et al. (2009), but account for the contributions from both the shear term and the emergence term. We found 17 of the 28 emerging ARs follow the hemisphere rule (61%), as shown in Fig. 5. This is consistent with Yang et al. (2009), except our sample is collected in the early phase of Solar Cycle 24 while theirs is in Cycle 23. It is not surprising because the method of Yang et al. (2009), though limited, still captures most of the helicity from the shear term, and the shear term contributes most of the helicity in the corona, as shown in the previous section. On the other hand, since the sample we used here is small, the

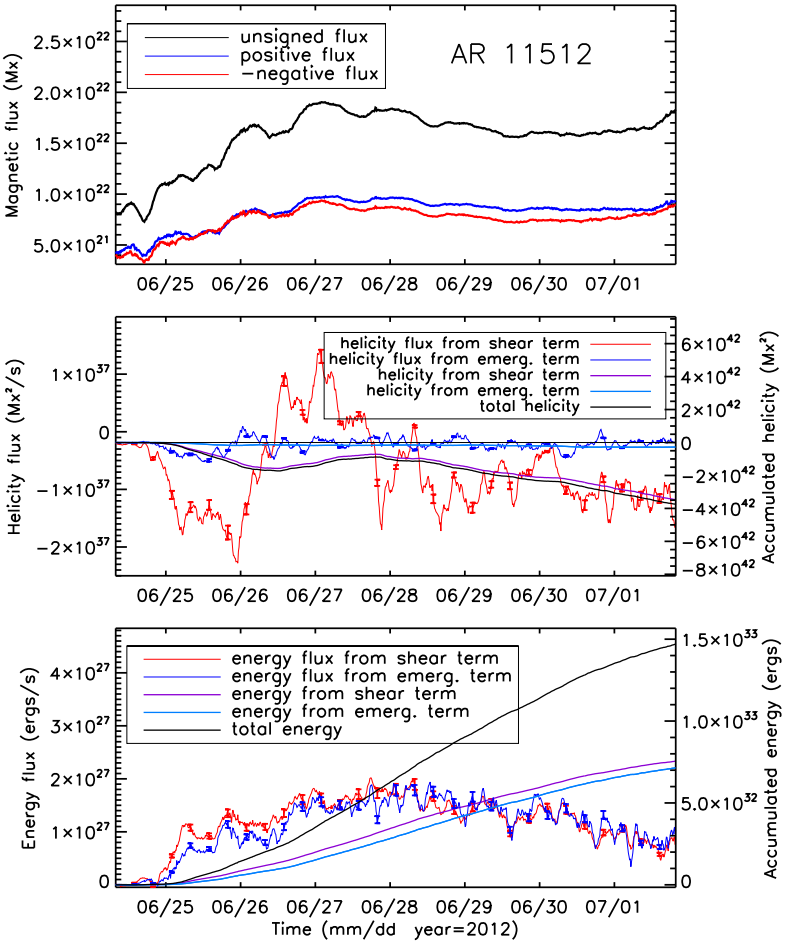

Fig. 4.— Same as Fig. 2 but for active region AR 11512.

hemisphere sign predominance is not statistically significant. At a 95% confidence interval, the result is $61\% \pm 18\%$. A larger sample is needed to repeat this test in future.

The hemisphere rule was also examined previously using the constant force-free α parameter to represent magnetic helicity in an AR (e.g. Seehafer 1990; Pevtsov et al. 1995; Hagino & Sakurai 2004; Tiwari et al. 2009; Zhang et al. 2010). This α is deemed to be a measure of magnetic twist in the AR, a fraction of magnetic helicity. Here we repeat the hemisphere rule test using the constant force-free α parameter.

Determining a constant α to represent the global magnetic twist of an AR is a challenge, because computing α involves calculating the derivative of a noisy tangential magnetic field.

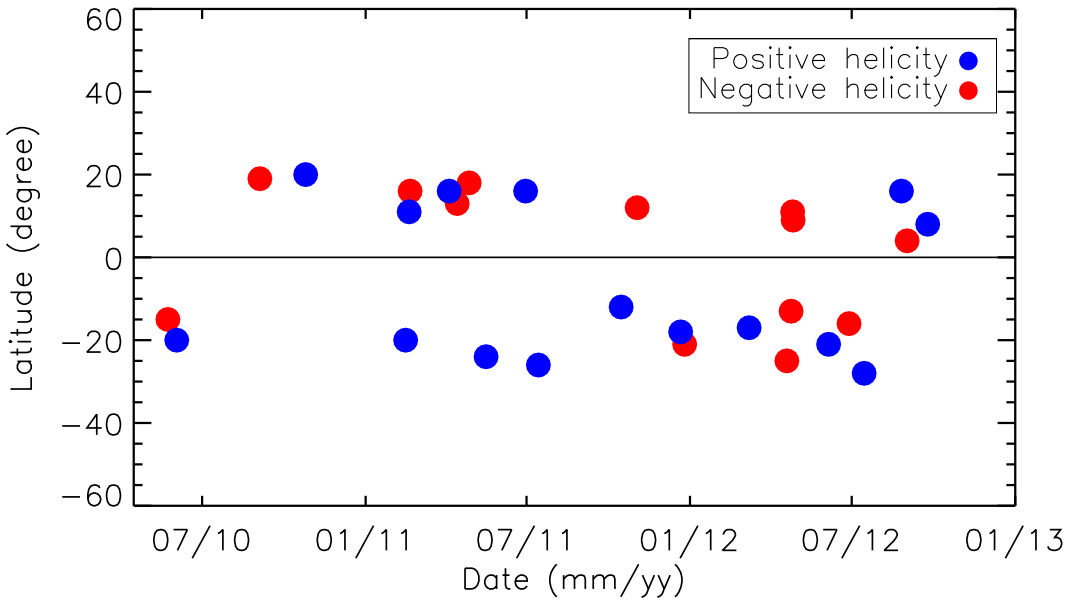

Fig. 5.— Distribution of the sign of magnetic helicity in emerging ARs as a function of latitude and time for the early phase of Solar Cycle 24 from May 2010 to September 2012. 61% ± 18% of 28 emerging ARs follow the hemisphere rule.

Thus an α map for any given AR usually looks very noisy. Simply averaging α over the region might be sensitive to data noise. Sometimes an α map may even contain mixed signs in sunspots (e.g. Su et al. 2009). Efforts have been made to search for a better method for determining a constant force-free α for an AR (e.g. Pevtsov et al. 1995; Hagino & Sakurai 2004; Tiwari et al. 2009). Leka & Skumanich (1999) evaluated three methods for deriving the constant α from observed vector magnetograms in ARs. These methods are based on (1) the distribution of α, (2) a least-squares fit to current and magnetic field, and (3) matching the observed horizontal field. They found that "the resulting value of the α parameters is often consistent within the uncertainties," and, if the calculation is restricted to 3σ of measurements, the three methods tested lead to "fairly quantitative agreement." They further found that one of the most robust approaches is to calculate the weighted mean of α. The winding rate in twisted flux tubes inferred from the vector magnetic field at the photosphere is also tested with simulation data (Crouch 2012).

In this study, we use a weighted mean of α, as proposed by Hagino & Sakurai (2004),

as the measure of global twist in an AR:

$$\alpha_{av} = \frac{\int_S \alpha(x,y) B_z^2(x,y) dxdy}{\int_S B_z^2(x,y) dxdy}, \tag{5}$$

where B_z is the vertical component of magnetic field. One advantage of α_{av} over nominal average force-free α calculations is that the singularities at the polarity inversion lines are avoided (Tiwari et al. 2009).

We calculate α_{av} for each AR directly using Eq. 5. This calculation is carried out using the 24 hours of vector magnetic field data, taken at a 12-minute cadence, after an AR's emergence has apparently ended. For each AR, we then take the median of those values. The end of the emergence of an AR is defined as (1) after the main emergence process, during which the total magnetic flux increases rapidly, and (2) when the increase of the total magnetic flux, if applied, is small in comparison to the increase of the magnetic flux in the main emergence process. This date is denoted in Column 7 of Table 1. For each data set, only strong-field pixels, or those with a magnetic field strength greater than 300 Mx cm^{-2} (roughly 3σ of field strength), are used in the computation (Hoeksema et al. 2013). Thus this meets two basic requirements for a reasonably reliable method for calculating α found by Leka & Skumanich (1999): (1) a weighted mean of α, and (2) a calculation restricted to 3σ of measurements. In this test, we found 57% ± 18% (16 of the 28) of ARs follow the hemisphere rule, slightly less than that when using the helicity (61% ± 18%). This minor discrepancy is not significant because the sample used is small. The criteria for choosing the end date for computation are qualitative; however, because the constant force-free α for an emerging AR is roughly constant after emergence (Pevtsov et al. 2003), this selection does not lead to bias in this test. Indeed, the signs of the daily median of the α_{av} for each AR after its emergence have the same sign in the sample analyzed here.

Magnetic twist in flux tubes can be acquired during their rise through the convection zone (CZ). Two scenarios have been proposed to interpret the hemisphere rule of magnetic twist: the Coriolis force acting on a rising flux tube (e.g. Holder et al. 2004), and the Σ-effect (Longcope et al. 1998). In the Coriolis force scenario, the force tilts one leg of the tube toward the equator and the other away. This deformation generates magnetic writhe, or a measure of the helical distortion of the tube's central axis, in the tube. In order to conserve helicity, the same amount of twist is produced within the tube, but with the opposite sign. The sign of the twist follows the hemisphere rule (Longcope et al. 1998; Holder et al. 2004). In the Σ-effect scenario (Longcope et al. 1998), a flux tube is buffeted by the turbulence of convection outside of the tube during its rise through the CZ. The convective turbulence has a non-zero kinetic helicity, which causes the tube to deform. This deformation produces

magnetic writhe in the tube, and the same amount of magnetic twist of opposite sign must be generated in the tube. The sign of the resulting twist is consistent with the hemisphere rule. Although both scenarios can explain the hemisphere rule of the twist, they fail to explain the hemisphere rule of the helicity, because the helicity actually includes both twist and writhe. The aforementioned mechanisms produce the same amount of twist and writhe of opposite signs, and they cancel out completely. If the helicity in ARs shows a hemisphere preference, it implies that this helicity is likely to be generated by the dynamo process, which has been suggested by Seehafer (1996), Ruzmaikin (1996), and Berger & Ruzmaikin (2000). More samples are needed to examine the hemisphere preference of the helicity. This will help test the dynamo-process hypothesis.

A third possible helicity source related to the rise of a tube is that twist comes from the background poloidal field wrapping around the rising flux tube as it passes through the CZ (Choudhuri Scenario, Choudhuri 2003; Choudhuri et al. 2004). The twist follows the usual sign rule during most of each solar cycle; however, this scenario also predicts a reversal of the hemisphere rule at the beginning of the solar cycle – this is due to the phase relation between the toroidal and poloidal fields generated by Babcock-Leighton type dynamo models. The sample of 28 ARs mentioned above does not exhibit a reversal of the hemisphere rule of magnetic twist: 57% ± 18% of ARs follow the hemisphere rule. Since those data are within the years 2010 – 2013, the beginning of Solar Cycle 24, this does not strongly support Choudhuri Scenario.

4.2. Discussion

4.2.1. Relationship between the signs of the helicity and twist in emerging ARs

As discussed in the previous section, testing the hemisphere rule has been done in some investigations using constant force-free α. It is worthwhile to examine how well the signs between this proxy of helicity and the helicity itself agree (or disagree). We do this test using the sample of 28 ARs described in Section 2. α_{av} is computed from one day of vector magnetic field data, taken at a 12-minute cadence, after an AR's emergence has apparently ended (Column 7 of Table 1). Fig. 6 is a scatter plot relating the helicity and α_{av}. The α_{av} plotted in Fig. 6 is the median of the α_{av} computed from this one day of data. The error bars represent the standard deviation of the α_{av} from the day of data[3]. The helicity, plotted

[3]The error of α_{av} is also estimated using a Monte Carlo simulation. In this test, we randomly add noise to the three components of magnetic field — B_x, B_y, and B_z — and then compute α_{av}. The noise has a Gaussian distribution with a width (or standard deviation) of 100 Mx cm^{-2}, roughly one σ of the field

on the y-axis, is the integral over time of both helicity-flux terms during the entire course of the active region's emergence. A Monte Carlo simulation carried out in Liu & Schuck (2012) indicates that the error in helicity flux calculated from HMI vector magnetograms is about 23%. The error in the helicity, shown as error bars in Fig. 6, is computed from this flux error (very small)[4]. The relationship of the signs between the helicity and the twist (inferred by α_{av}) is reasonably strong: 25 of the 28 ARs have the same sign, i.e., $89\% \pm 11\%$ at a 95% confidence interval.

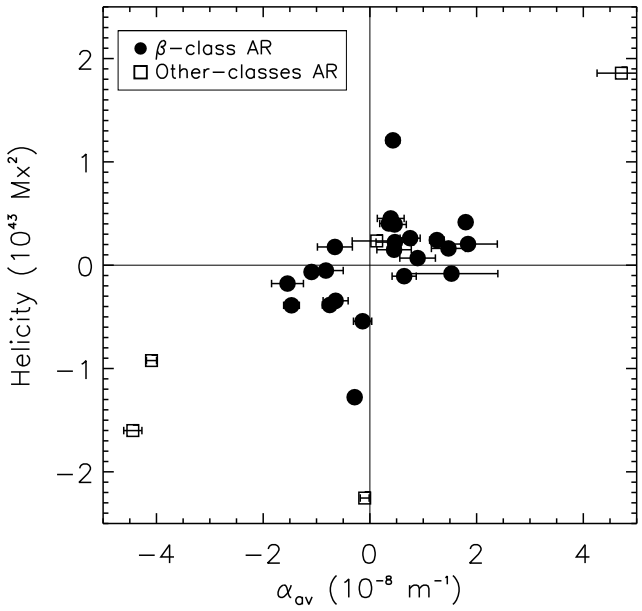

Fig. 6.— Comparison between the helicity (y-axis) and α_{av} (x-axis). 25 in a sample of 28 emerging ARs (89% ± 11%) have the same sign. Dot denotes Hale's β class ARs; square denotes other classes.

strength of the HMI vector field data. The experiment was repeated 2000 times. We randomly selected 15 ARs, roughly half of the ARs in the sample. The error ranges between 5% to 35% for a single α_{av} measurement. Averaging one day of α_{av} together yields an error of about 2% on average, much smaller than the errors reported in Fig 6.

[4]We also take another approach to estimate the uncertainty in the helicity. First, for each helicity flux density map we choose a small area (20×20 pixels) at the bottom left corner of the map in the quiet Sun region. Then, we compute the median of the absolute values of the helicity flux density in this area. This median is deemed to be the error of the helicity flux density. This error is then propagated to derive the error of the helicity flux at that time. Finally, the error of the helicity is calculated. This error is small, about two orders of magnitude lower than the helicity, comparable to the errors from the Monte Carlo simulation.

4.2.2. Examining the relationship between magnetic twist and size of the flux tube

Flux emergence models predict a relationship between the size of the AR flux tube and the twist in the tube: twist depends on r^{-2}, where r is the radius of the flux tube, i.e., there will be greater twist in smaller flux tubes (e.g. Longcope et al. 1998; Choudhuri et al. 2004). These studies motivate examining a general relationship between twist and active region size. Plotted in Fig. 7 are scatter plots of $\mid \alpha_{av} \mid$, the absolute value of α_{av}, versus r^{-2} for the whole sample of 28 emerging ARs (left) and for the 23 ARs in the sample that have a Hale's β class magnetic configuration (right). An β class AR is defined as a sunspot group having both positive and negative magnetic polarities (bipolar), with a simple and distinct division between the polarities (Hale et al. 1919). Thus this class of AR is deemed to have a simple bipolar configuration. For each AR, the plot shows the median value and standard deviation of the α_{av} computed from one day of vector magnetic field data, taken at a 12-minute cadence, after the emergence of the AR has apparently ended, as described in Section 2. Only pixels with a field strength greater than 300 Mx cm^{-2} are used for the computation. r is computed by measuring the total size of these strong-field pixels. More specifically, $r = (0.5 \times n \times l^2)^{0.5}$, where n refers to the number of the strong-field pixels and l is pixel size. The right panel of Fig. 7 suggests that smaller active regions can support higher twist in agreement with the general predictions of the thin flux-tube models. This is illustrated by the dashed line at $r^{-2} = 8.8 \times 10^{-8} \mid \alpha_{av} \mid$, drawn to place the majority of the data to the left of the line while accounting for the 1-σ error bars of the two outliers.

5. Conclusions

We used HMI vector magnetic field data to study magnetic helicity in 28 emerging ARs that appeared on the solar disk from May 2010 to September 2012, the early phase of Solar Cycle 24. The HMI observations cover the entire course of emergence of these ARs. Helicity in an AR is calculated by integrating over time the helicity flux across the photosphere, which is comprised of two terms: the emergence term that advects the twisted magnetic field into the corona and the shear term that shears magnetic field by photospheric motions. In most ARs (26 of 28) both terms contribute the same sign helicity and in all cases the magnitude of shear term is dominant. The emergence term contributes about 14% of the helicity on average in a sample of 26 emerging ARs. (The two ARs in which the two terms inject opposite sign helicities are excluded in this average. However, the shear term in those two ARs is also dominant in magnitude, contributing the most helicity.) Both terms, on the other hand, contribute approximately equally to the energy in the corona (including potential energy and free energy), with the emergence term contributing slightly more, about 56% on

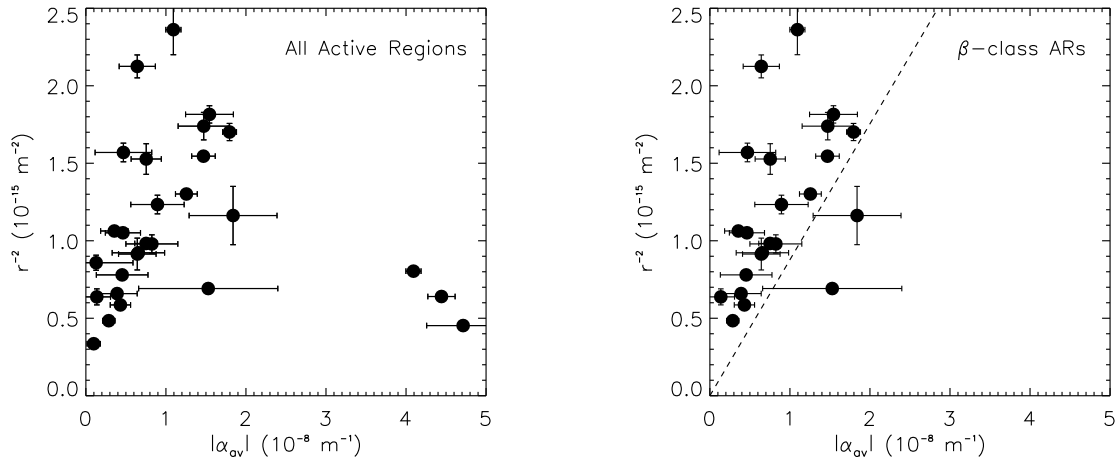

Fig. 7.— Relationship between flux tube size and twist. r refers to size of the AR flux tube. $\mid \alpha_{av} \mid$ denotes a measure of the magnitude of magnetic twist in ARs. Left: r^{-2} versus $\mid \alpha_{av} \mid$ for the whole sample of 28 emerging ARs. Right: only emerging ARs with a β-class magnetic configuration are included (23 ARs). The dashed line in the right, $r^{-2} = 8.8 \times 10^{-8} \mid \alpha_{av} \mid$, drawn to place the majority of the data to the left of the line while accounting for the 1-σ error bars of the two outliers, suggests a possible AR-size dependent threshold of magnetic twist in β-class ARs.

average.

17 of the 28 emerging ARs (61% ± 18%) follow the hemisphere rule of magnetic helicity, negative in the north and positive in the south. As the sample is small, this result is unable to confirm this hemisphere rule statistically. More data are needed.

The signs of the magnetic helicity and twist in ARs are studied. In 89% ± 11% of the 28 emerging ARs the magnetic helicity and magnetic twist, measured by a constant force-free α_{av}, have the same sign. An upper limit of magnetic twist that depends on the size of solar ARs is inferred from a sample of 23 ARs that have a bipolar magnetic field configuration.

Table 1. Emerging ARs analyzed in this work.

NOAA	Lat.[a] (^{o})	Start Date/Time[b] (yyyy.mm.dd/hh:mm:ss)	Stop Date/Time[c] (yyyy.mm.dd/hh:mm:ss)	Emerg. Beginning[d] (yyyy.mm.dd/hh)	Emerg. End[e] (yyyy.mm.dd/hh)	Date[f] (yyyy.mm.dd)	Config.[g]
11072	S16	2010.05.20/00:00:00	2010.05.26/21:36:00	2010.05.20/12	2010.05.23/00	2010.05.23	β
11076	S27	2010.05.30/00:00:00	2010.06.05/20:36:00	2010.05.30/19	2010.06.03/20	2010.06.04	β
11105	N18	2010.09.02/00:00:00	2010.09.05/23:36:00	2010.09.02/00	2010.09.05/11	2010.09.05	β
11117	N22	2010.10.23/00:00:00	2010.10.27/23:36:00	2010.10.23/00	2010.10.25/22	2010.10.25	β
11158	S21	2011.02.12/00:00:00	2011.02.17/23:36:00	2011.02.12/00	2011.02.14/20	2011.02.15	$\beta\gamma$
11161	N12	2011.02.15/00:00:00	2011.02.22/23:36:00	2011.02.15/00	2011.02.17/10	2011.02.18	$\beta\gamma$
11162	N18	2011.02.17/00:00:00	2011.02.22/23:36:00	2011.02.17/20	2011.02.20/21	2011.02.21	β
11184	N16	2011.04.02/00:00:00	2011.04.07/23:36:00	2011.04.02/16	2011.04.06/18	2011.04.07	β
11190	N13	2011.04.10/00:00:00	2011.04.17/23:36:00	2011.04.10/12	2011.04.16/22	2011.04.17	$\beta\gamma$
11199	N18	2011.04.25/00:00:00	2011.04.29/23:36:00	2011.04.25/14	2011.04.29/08	2011.04.29	β
11214	S24	2011.05.13/00:00:00	2011.05.19/23:36:00	2011.05.13/15	2011.05.17/20	2011.05.18	β
11242	N16	2011.06.28/00:00:00	2011.07.02/00:36:00	2011.06.29/01	2011.06.30/19	2011.07.01	β
11250	S27	2011.07.10/00:00:00	2011.07.18/18:36:00	2011.07.10/01	2011.07.14/08	2011.07.15	β
11316	S12	2011.10.11/00:00:00	2011.10.19/23:36:00	2011.10.11/06	2011.10.14/10	2011.10.17	β
11334	N11	2011.10.30/00:00:00	2011.11.05/23:36:00	2011.10.30/00	2011.11.01/05	2011.11.03	β
11382	S14	2011.12.17/00:00:00	2011.12.25/23:36:00	2011.12.18/04	2011.12.21/20	2011.12.22	β
11385	S34	2011.12.24/00:00:00	2011.12.27/23:36:00	2011.12.24/15	2011.12.27/15	2011.12.27	β
11428	S17	2012.03.03/00:00:00	2012.03.11/23:36:00	2012.03.03/00	2012.03.07/01	2012.03.08	β
11462	S25	2012.04.16/00:00:00	2012.04.21/23:36:00	2012.04.17/12	2012.04.20/20	2012.04.21	β
11465	S19	2012.04.19/12:00:00	2012.04.27/23:36:00	2012.04.19/17	2012.04.24/02	2012.04.25	$\beta\gamma\delta$
11466	N12	2012.04.22/00:00:00	2012.04.28/23:24:00	2012.04.22/00	2012.04.24/02	2012.04.25	β
11468	N8	2012.04.24/00:00:00	2012.04.27/23:36:00	2012.04.24/00	2012.04.26/12	2012.04.27	β
11497	S21	2012.06.01/00:00:00	2012.06.08/21:36:00	2012.06.01/00	2012.06.07/18	2012.06.08	β
11512	S16	2012.06.24/00:00:00	2012.07.01/21:36:00	2012.06.24/18	2012.06.28/12	2012.06.30	β
11523	S28	2012.07.11/00:00:00	2012.07.18/21:36:00	2012.07.11/20	2012.07.15/20	2012.07.16	β
11554	N16	2012.08.23/00:00:00	2012.08.28/21:36:00	2012.08.23/08	2012.08.25/06	2012.08.26	β
11560	N3	2012.08.29/00:00:00	2012.09.04/16:48:00	2012.08.29/10	2012.09.02/18	2012.09.03	$\beta\gamma$
11577	N8	2012.09.22/00:00:00	2012.09.26/23:36:00	2012.09.22/00	2012.09.23/08	2012.09.23	β

[a]The latitude of the AR studied. "N" refers to northern hemisphere, and "S" to southern.

[b]Starting time of the time interval in which the data are used for this AR.

[c]Stopping time of the time interval in which the data are used.

[d]The instance when the AR begins to quickly emerge.

[e]The instance when emergence of the AR ends.

[f]The date in which the data are used to compute the average of α_{av} and r in Figs. 6 and 7.

[g]Hale's classification of the magnetic configuration of the AR (Hale et al. 1919) on the date listed in Column 7.

We wish to thank the team members who have made great contributions to the SDO mission for their hard work! We thank the anonymous referee for comments and suggestions that improved the paper. This investigation was supported by NASA Contract NAS5-02139 (HMI) to Stanford University and by NASA LWS and HGI grants.

REFERENCES

Abramenko, V. I., Wang, T., & Yurchishin, V. B. 1996, Sol. Phys., 168, 75

Bao, S., & Zhang, H. 1998, Astrophys. J., 496, L43

Berger, M. A. 1984, Geophysical & Astrophysical Fluid Dynamics, 30, 79

—. 1985, Astrophy. J. Supp. Ser., 59, 433

Berger, M. A., & Field, G. B. 1984, J. Fluid Mech., 147, 133

Berger, M. A., & Ruzmaikin, A. 2000, Journal of Geophysical Research, 105, 10481

Borrero, J. H., Tomczyk, S., Kubo, M., Socas-Navarro, H., Schou, J., Couvidat, S., & Bogart, R. 2011, Sol. Phys., 273, 267

Choudhuri, A. R. 2003, Sol. Phys., 215, 31

Choudhuri, A. R., Chatterjee, P., & Nandy, D. 2004, Astrophys. J., 615, L57

Crouch, A. D. 2012, Sol. Phys., 281, 669

Démoulin, P. 2007, Advances in Space Research, 39, 1674

Démoulin, P., & Berger, M. A. 2003, Sol. Phys., 215, 203

Fan, Y. 2009, Living Reviews in Solar Physics, 6

Georgoulis, M. K., & LaBonte, B. J. 2007, Astrophys. J., 671, 1034

Gilman, P. A. 1983, Astrophys. J. S., 53, 243

Hagino, M., & Sakurai, T. 2004, Publications of the Astronomical Society of Japan, 56, 831

Hale, G. E., Ellerman, F., Nicholson, S. B., & Joy, A. H. 1919, Astrophys. J., 49, 153

Hao, J., & Zhang, M. 2011, Astrophys. J., 733, L27

Hoeksema, J. T., et al. 2013, Sol. Phys., to be submitted

Holder, Z. A., Canfield, R. C., McMullen, R. A., Nandy, D., Howard, R. F., & Pevtsov, A. A. 2004, Astrophys. J., 611, 1149

Kusano, K., Maeshiro, T., Yokoyama, T., & Sakurai, T. 2002, Astrophys. J., 577, 501

LaBonte, B. J., Georgoulis, M. K., & Rust, D. M. 2007, Astrophys. J., 671, 955

Leka, K. D., Barnes, G., Crouch, A. D., Metcalf, T. R., Gary, G. A., Jing, J., & Liu, Y. 2009, Sol. Phys., 260, 83

Leka, K. D., & Skumanich, A. 1999, Sol. Phys., 188, 3

Liu, Y., & Schuck, P. W. 2012, Astrophys. J., 761, article id. 105

Longcope, D. W., Fisher, G. H., & Pevtsov, A. A. 1998, Astrophys. J., 507, 417

Longcope, D. W., & Welsch, B. T. 2000, Astrophys. J., 545, 1089

Metcalf, T. R. 1994, Sol. Phys., 155, 235

Metcalf, T. R., et al. 2006, Sol. Phys., 237, 267

Nindos, A., Zhang, J., & Zhang, H. 2003, Astrophys. J., 594, 1033

Norton, A. A., et al. 2006, Sol. Phys., 239, 69

Pariat, E., Démoulin, P., & Berger, A. A. 2005, Astronomy and Astrophysics, 439, 1191

Pevtsov, A. A., & Balasubramaniam, K. S. 2003, Advances in Space Research, 32, 1867

Pevtsov, A. A., Canfield, R. C., & Metcalf, T. R. 1995, Astrophys. J., 440, L109

Pevtsov, A. A., Maleev, V. M., & Longcope, D. W. 2003, Astrophys. J., 593, 1217

Ruzmaikin, A. A. 1996, Geophysical Research Letters, 23, 2649

Scherrer, P. H., et al. 1995, Sol. Phys., 162, 129

—. 2012, Sol. Phys., 275, 207

Schou, J., et al. 2012, Sol. Phys., 275, 229

Schuck, P. W. 2008, Astrophys. J., 683, 1134

Seehafer, N. 1990, Sol. Phys., 125, 219

—. 1996, Physical Review E, 53, 1283

Snyder, J. P. 1987, Map projections–A working manual No. 1395 (USGPO)

Su, J. T., Sakurai, T., Suematsu, Y., Hagino, M., & Liu, Y. 2009, Astrophys. J. L., 697, L103

Sun, X. 2013, ArXiv e-prints

Tiwari, S. K., Venkatakrishnan, P., Gosain, S., & Joshi, J. 2009, Astrophys. J., 700, 199

Turmon, M., Jones, H. P., Malanushenko, O. V., & Pap, J. M. 2010, Sol. Phys., 262, 277

Yamamoto, T. T., & Sakurai, T. 2009, Astrophys. J., 698, 928

Yang, S., Zhang, H., & B*ü*chner, J. 2009, A. Ap., 502, 333

Zhang, H., Sakurai, T., Pevtsov, A., Gao, Y., Xu, D., Sokoloff, D. D., & Kuzanyan, K. 2010, Monthly Notices of the Royal Astronomical Society, 402, L30

Zhang, H., & Yang, S. 2013, Astrophys. J., 763